All-*Trans* Retinol in Rod Photoreceptor Outer Segments Moves Unrestrictedly by Passive Diffusion

Qingqing Wu,*† Chunhe Chen,* and Yiannis Koutalos*
*Department of Ophthalmology, Medical University of South Carolina, Charleston, South Carolina; and †Department of Nephrology, First Affiliated Hospital of Sun Yat-sen University, Guangzhou, People's Republic of China

ABSTRACT The visual pigment protein of vertebrate rod photoreceptors, rhodopsin, contains an 11-*cis* retinyl moiety that is isomerized to all-*trans* upon light absorption. Subsequently, all-*trans* retinal is released from the protein and reduced to all-*trans* retinol, the first step in the recycling of rhodopsin's chromophore group through the series of reactions that constitute the visual cycle. The concentration of all-*trans* retinol in photoreceptor outer segments can be monitored from its fluorescence. We have used two-photon excitation (720 nm) of retinol fluorescence and fluorescence recovery after photobleaching to characterize the mobility of all-*trans* retinol in frog photoreceptor outer segments. Retinol produced after rhodopsin bleaching moved laterally in the disk membrane bilayer with an apparent diffusion coefficient of $2.5 \pm 0.3\ \mu m^2\ s^{-1}$. The diffusion coefficient of exogenously added retinol was $3.2 \pm 0.5\ \mu m^2\ s^{-1}$. These diffusion coefficients are in close agreement with those reported for lipids, suggesting that retinol is not tightly bound to protein sites that would be diffusing much more slowly in the plane of the membrane. In agreement with this interpretation, a fluorescent-labeled C-16 fatty acid diffused laterally with a similar diffusion coefficient, $2.2 \pm 0.2\ \mu m^2\ s^{-1}$. Retinol also moved along the length of the rod outer segment, with an apparent diffusion coefficient of $0.07 \pm 0.01\ \mu m^2\ s^{-1}$, again suggesting that it is not tightly bound to proteins that would confine it to the disks. The axial diffusion coefficient of exogenously added retinol was $0.05 \pm 0.01\ \mu m^2\ s^{-1}$. In agreement with passive diffusion, the rate of axial movement was inversely proportional to the square of the length of the rod outer segment. Diffusion of retinol on the plasma membrane of the outer segment can readily account for the measured value of the axial diffusion coefficient, as the plasma membrane comprises ~1% of the total outer-segment membrane. The values of both the lateral and axial diffusion coefficients are consistent with most of the all-*trans* retinol in the outer segments moving unrestricted and not being bound to carrier proteins. Therefore, and in contrast to other steps of the visual cycle, there does not appear to be any specialized processing for all-*trans* retinol within the rod outer segment.

INTRODUCTION

Detection of light by vertebrate rod photoreceptor cells takes place in the outer-segment compartment and begins with the isomerization of the chromophore of the visual pigment, rhodopsin, from 11-*cis* to all-*trans*. The bleached rhodopsin then has to be regenerated with 11-*cis* retinal for the cell to regain its pigment complement and light sensitivity. The first steps in this regeneration process consist of the release of the chromophore all-*trans* retinal from the bleached rhodopsin and its reduction to all-*trans* retinol by retinol dehydrogenase. All-*trans* retinol is transported out of the rod outer segment to the neighboring retinal pigment epithelial cells and, through a series of reactions, remade into 11-*cis* retinal. The 11-*cis* retinal is brought back to the outer segment, where it combines with the visual pigment protein moiety to reform rhodopsin. The process of visual pigment bleaching and regeneration comprises the visual cycle (1–3).

The refashioning of 11-*cis* retinal through the visual cycle involves a series of chemical intermediates, as well as transport between different cells and within cellular compartments. After release from photoactivated rhodopsin, all-*trans* retinal is reduced to all-*trans* retinol by retinol dehydrogenase in a reaction requiring NADPH (4,5). Some of the all-*trans* retinal can be sequestered inside the disks, bound via a Schiff base to phosphatidylethanolamine (6). The phosphatidylethanolamine-all-*trans*-retinal compound is then transported to the cytoplasmic side by the ABCR transporter (6) and the sequestered all-*trans* retinal is made available for reduction. Although the aqueous solubility of all-*trans* retinol is very low (7), it can be readily removed from the outer segments of intact cells by lipophilic carriers (8), suggesting that retinol equilibrates rapidly between the cytoplasmic leaflet of the disk membrane and the outer leaflet of the plasma membrane. Equilibration between the inner and outer leaflets of the plasma membrane in particular should not present any problem, as retinol is an uncharged hydrophobic molecule. Fatty acids, for example, are known to equilibrate rapidly between the leaflets of membrane bilayers (9). The transport of retinol from the rod outer segment to the retinal pigment epithelial cells is thought to be facilitated by the interphotoreceptor retinoid binding protein (10,11), though the visual cycle remains mostly unperturbed in mice lacking the protein (12,13). In the retinal pigment epithelium, all-*trans* retinol is converted to retinyl ester (14), which is subsequently isomerized to 11-*cis* retinol (15,16). 11-*cis* retinol is then oxidized to 11-*cis* retinal, which is transported back to photoreceptor outer segments where it associates with opsin to reform rhodopsin. These last steps of the visual cycle involving 11-*cis* retinal are not understood in detail.

Submitted April 7, 2006, and accepted for publication September 14, 2006.

Address reprint requests to Dr. Yiannis Koutalos, Dept. of Ophthalmology, Medical University of South Carolina, 167 Ashley Ave., Charleston, SC 29425. Tel.: 843-792-9180; Fax: 843-792-4096; E-mail: koutalo@musc.edu.

0006-3495/06/12/4678/12 $2.00

doi: 10.1529/biophysj.106.086728

Thus, the regeneration of the visual pigment is accomplished through a specialized and highly intricate series of reactions and intermediates. Not much is known about the carriage of retinol within the rod outer segment itself, and its mobility has been the focus of investigations spanning several years. Previous studies (17,18) took advantage of the fluorescence of all-*trans* retinol to monitor its movement, whereas others (19) were based on its distinctive light absorption properties. Because of the technical limitations at the time, these studies were largely qualitative, but they did seem to indicate that the all-*trans* retinol produced locally after rhodopsin bleaching can move axially within the rod outer segment (18,19).

We have used two-photon excitation (720 nm) of retinol fluorescence to monitor the concentration of retinol in frog rod outer segments. We measured the mobility of all-*trans* retinol using fluorescence recovery after photobleaching (FRAP). The mobility measurements are consistent with the bulk of the all-*trans* retinol produced after rhodopsin bleaching moving unrestricted in the plane of the disk membranes as well as axially along the length of the rod outer segment. This is further supported by the observation that the mobility of retinol is virtually the same as that of a fluorescent C-16 fatty acid analog. We find then that there is no specialized processing of all-*trans* retinol within the rod outer segment, contrary to other intermediates and to the specialized transport for retinol itself between outer segment and retinal pigment epithelium.

MATERIALS AND METHODS

Living, isolated rod photoreceptors were obtained from grass frogs (*Rana pipiens*; NASCO, Fort Atkinson, WI) as described previously (20). An animal was sacrificed after being dark-adapted overnight, the eyes were enucleated, and the retinas were excised under infrared or dim red light (Kodak filter No. 2) and placed in amphibian Ringer's (in mmol/L: 110 NaCl, 2.5 KCl, 1.6 $MgCl_2$, 1 $CaCl_2$, 5 HEPES, 5 glucose, pH 7.55). Single photoreceptor cells were obtained by chopping the retina with a razor blade on Sylgard elastomer. Isolated cells were transferred to 100-μL chambers (glass-bottomed culture dishes from Warner Instruments, Hamden, CT) that fit on the microscope stage.

The isolation procedure results in three types of rod photoreceptor cells or fragments: intact cells, rod outer segments with attached ellipsoids (ROS-RIS), and rod outer segments (ROS). For experiments with endogenously produced retinol, only intact cells and ROS-RIS fragments were used, as those were the ones that could form retinol quantitatively and thereby had sufficiently high levels of fluorescence. In terms of retinol formation, the metabolic competence of ROS-RIS fragments is equivalent to that of intact cells (see Chen et al. (20); for general metabolic competence, see Biernbaum and Bownds (21)). In experiments with exogenously added retinol, metabolic competence for retinol formation was not a concern, so ROS were also used for comparison. In experiments measuring lateral mobility, no significant differences were observed in data obtained from intact cells or ROS-RIS, so the results have been combined, whereas the results from ROS are reported separately. The ROS-RIS fragments used included rounded and tapered inner segments. The inner and outer segments are fused in the case of rounded inner segments, allowing the free diffusion of rhodopsin between the two compartments (22). This communication between the two compartments is not expected to affect the measurements of lateral mobility on the outer-segment disk surfaces. Experiments measuring longitudinal mobility lasted significantly longer than those measuring lateral mobility, and were carried out exclusively with intact cells, as ROS-RIS fragments did not maintain their integrity for the length of the experiment. Although we did not test the spectral sensitivity of the cells, most of them are expected to be the rhodopsin-containing ''red'' rods, which comprise the overwhelming majority of the rod population in amphibian retinas (23). The morphology of the selected cells (larger outer-segment width) was generally consistent with them being of the ''red'' variety.

For measurements of endogenous retinol mobility, isolated cells were bleached with white light and kept in the dark for ~1 h. This procedure leads to the conversion of 80–90% of rhodopsin's chromophore to retinol, as measured with extraction of retinoids from whole frog retinas and high-performance liquid chromatography ((19); Wu, Robertson, Crouch and Koutalos, unpublished). Because retinol outer-segment levels decrease slowly over time, retinol mobility measurements were carried out within the following 1–2 h. For measurements with high levels of exogenous retinol, the same procedure was followed, but during the 1 h in the dark the cells were incubated with 100 μmol/L all-*trans* retinol, and subsequently washed three to four times with Ringer's to remove excess retinol. As judged by the levels of retinol fluorescence, this treatment resulted in outer-segment retinol concentrations that were 5–10 times higher than the endogenous. For measurements with low, physiological levels of exogenous retinol, the whole retina was bleached, and the endogenous retinol was removed by incubating the retina for 1 h with 1% lipid free bovine serum albumin (BSA). Afterwards, single photoreceptor cells were obtained by chopping the retina with a razor blade. Isolated cells were transferred to 100-μL chambers, incubated with 100 μmol/L all-*trans* retinol for 10–15 min, and subsequently washed three to four times with Ringer's to remove excess retinol. We judged the levels of the exogenous retinol in cells by comparing its fluorescence with that of endogenous retinol from control cells. For measurements with 4, 4-difluoro-5,7-dimethyl-4-bora-3a,4a-diaza-*s*-indacene-3-hexadecanoic acid (BODIPY FL C_{16}, Molecular Probes, Eugene, OR), bleached cells were incubated for 30 min with 1 μmol/L dye; excess dye was removed by washing three to four times with Ringer's.

Retinol fluorescence was excited with 720 nm light (two-photon excitation, with 860 mW power at 720 nm) from a Ti:Sapphire tunable infrared (IR) laser (20,24) through a Zeiss 63× water immersion lens (NA = 0.9); fluorescence emission was collected from 400 to 650 nm. BODIPY fluorescence was excited with 488 nm light from an Argon laser (25 mW), and its emission was collected from 505 to 700 nm. BODIPY measurements were carried out in a nonconfocal mode, with the pinhole fully open (1000 μm), allowing a precise definition of the cell area from which fluorescence was collected (see below and Fig. 2 *A*) The lasers are part of a Zeiss LSM 510 Non-Linear Optical Confocal Microscope (Carl Zeiss, Thornwood, NY), which includes a 32-channel photomultiplier-tube array of detectors allowing the measurement of fluorescence emission spectra (Zeiss 510 Meta system).

We characterized the two-photon excitation properties of the imaging system with the particular lens and excitation wavelength by measuring the point-spread functions in the vertical direction z and in the horizontal directions x and y. The point-spread functions in the different directions were determined with 0.1 μm diameter fluorescent spheres (Molecular Probes) by measuring the fluorescence at different heights, z, and distances x and y. The fluorescence data from the spheres were fitted with Gaussian point-spread functions, $P(x)$, $P(y)$, and $P(z)$. For the x direction, for example, $P(x) \propto \exp\left(-x^2/2\sigma_x^2\right)$, with $P(x)$ the fluorescence intensity at distance x from the center of the sphere, and σ_x the standard deviation of the Gaussian function. Fig. 1 shows representative fluorescence intensity profiles in the three different directions for one particular sphere, along with the respective Gaussian function fits. Based on the results from 10 spheres, the fluorescence excitation properties of the imaging system in the three different directions were described by $\sigma_x = 0.27 \pm 0.01$ μm, $\sigma_y = 0.30 \pm 0.00$ μm, and $\sigma_z = 0.94 \pm 0.02$ μm (mean ± SE, $n = 10$). It is important to note that the extent of fluorescence excitation in the vertical direction z is a fraction of the diameter of the rod outer segments: the typical outer-segment diameter is ~6 μm, whereas the width at half-maximum for excitation is ~2 μm (2.21 ± 0.06 μm (mean ± SE)).

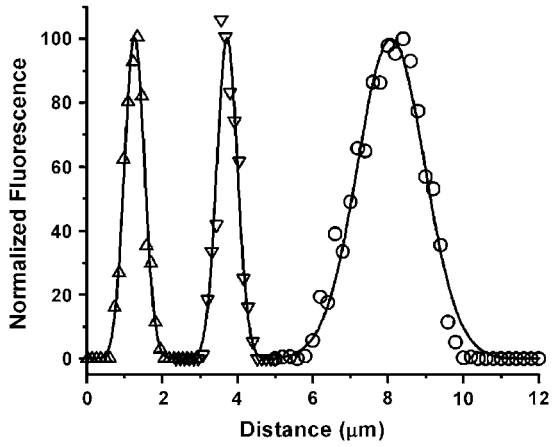

FIGURE 1 Two-photon imaging system point-spread functions, obtained with a fluorescent 0.1-μm sphere. Fluorescence intensity values in the x ($\triangle$), y ($\triangledown$), and z ($\bigcirc$) directions are plotted as a function of distance, each peak value corresponding to the center of the intensity profile in that axis. Gaussian curve fits and data points have been scaled to the same peak amplitude. The curve fits gave: $\sigma_x = 0.26$ μm, $\sigma_y = 0.27$ μm, and $\sigma_z = 0.89$ μm. Fluorescence excitation: 720 nm; fluorescence emission: 400-650 nm; lens: water-immersion, 63×, NA = 0.9.

For FRAP experiments, a high intensity of the appropriate laser beam was used for bleaching (35% and 40% of the full intensities at 720 and 488 nm, respectively), and a lower, non-bleaching intensity (3% and 1% of the full intensities at 720 and 488 nm, respectively) was used for scanning and measuring the distribution of fluorescence before and after bleaching. The intensities used for scanning did not cause any measurable bleaching after 20 scans. After bleaching, images were acquired at regular intervals and were subsequently analyzed with the Zeiss LSM510 system software or with ImageJ (http://rsb.info.nih.gov/ij/). Routine checks of emission spectra with the Meta detector array confirmed that the fluorescence recovery was due to retinol. All-*trans* retinal is also present in the outer segments under the conditions of the experiment, but its fluorescence quantum yield is <2% that of retinol (see Fig. 1 *B* in Tsina et al. (8)) and its concentration is <25% that of retinol (based on retinoid extractions, see above). Thus, the contribution of all-*trans* retinal to the observed fluorescence is negligible, as it should be <0.5% that of retinol.

An important consideration regarding the two-photon excitation measurements of retinol fluorescence was cell damage, especially because of the use of high laser intensities for FRAP experiments. High laser intensities can result in cell damage, as judged by significant changes in cell appearance, either because of heating or because of phototoxicity. We optimized the laser intensities used for scanning and bleaching so that they would not damage the cells, but would be adequate for reliable measurements.

All reagents were of analytical grade. Retinol was delivered to the cells using 1% BSA as carrier. We use BSA because we have found it to be an effective carrier for delivering retinoids to intact cells. BSA was washed away after loading and was not present during experiments. BODIPY FL C_{16} was prepared as 10 mM stock in dimethyl sulfoxide (DMSO) and diluted in Ringer's just before the cell incubations. The DMSO concentration during the incubation was 0.01%. DMSO was removed along with excess dye during the washes at the end of the incubation and was not present during experiments. All experiments were carried out at room temperature.

Analysis of lateral diffusion

For lateral diffusion of the fluorophores on the plane of the disk membrane, equilibration was rapid and it was possible to fit the fluorescence recovery data with simple exponentials, providing the fluorescence recovery rates. These rates, along with the diameter of the outer segment were used to obtain the apparent diffusion coefficient for the lateral mobility of the fluorophore. To a first approximation, the lateral diffusion coefficient, D, is given by

$$D = d^2 \times \frac{k}{\pi^2}, \tag{1}$$

where k is the rate of fluorescence recovery reflecting the rate of equilibration through diffusion and $d = 2R$ is the diameter of a disk, which is approximately the same as that of the outer segment (25). Eq. 1 provides an estimate of the lateral diffusion coefficient that is independent of the area that was bleached and the area over which the recovery was measured. In general, however, the recovery rate depends both on the bleaching pattern and the measuring area. Because in two-photon FRAP the experimental bleaching and measuring areas are not known accurately, we have examined the validity of lateral diffusion coefficients estimated through Eq. 1 using computer simulations. Diffusion on the surface of a rod outer-segment disk is described in cylindrical coordinates by

$$\frac{\partial c}{\partial t} = D \times \left(\frac{\partial^2 c}{\partial r^2} + \frac{1}{r} \times \frac{\partial c}{\partial r} + \frac{1}{r^2} \times \frac{\partial^2 c}{\partial \theta^2}\right), \tag{2}$$

where $c = c(r,\theta,t)$ is the concentration of the fluorophore at distance r from the center of the disk, angle θ, and time t. As there is no flux of the fluorophore at the edge of the disk, at $r = R$, the boundary condition is

$$\left.\frac{\partial c}{\partial r}\right|_{r=R} = 0. \tag{3a}$$

The initial concentration of the fluorophore on the disk reflects the bleaching pattern. If at $t = 0$

$$c(r,\theta,0) = u(r,\theta), \tag{3b}$$

the solution to Eq. 2 with boundary and initial conditions given by Eqs. 3a and 3b, respectively, is provided by ((26); see section 7.12, Problem II, p. 211))

$$c(r,\theta,t) = c_\infty + \sum_{s=1}^{\infty}\sum_{n=0}^{\infty}(A_{n,s} \times \cos n\theta + B_{n,s} \times \sin n\theta) \times J_n(\beta_s r/R) \times e^{-\beta_s^2 Dt/R^2}, \tag{4}$$

where

$$c_\infty = \frac{1}{\pi R^2} \times \int_0^R \int_{-\pi}^{\pi} u(r,\theta) \times r\,d\theta\,dr \tag{5a}$$

is the equilibrium concentration of the fluorophore on the disk surface, reached at long times after bleaching ((26); see section 7.8, Problem II, p. 204), and

$$A_{0,s} = \frac{1}{\pi R^2 \times \{J_0(\beta_s)\}^2} \times \int_0^R \int_{-\pi}^{\pi} u(r,\theta) \times J_0(\beta_s r/R) \times r\,d\theta\,dr, \tag{5b}$$

$$B_{0,s} = 0, \tag{5c}$$

whereas for integer $n > 0$,

$$A_{n,s} = \frac{2\beta_s^2}{\pi R^2 \times (\beta_s^2 - n^2)\{J_n(\beta_s)\}^2} \times \int_0^R \int_{-\pi}^{\pi} u(r,\theta) \times \cos n\theta \times J_n(\beta_s r/R) \times r\,d\theta\,dr \tag{5d}$$

and

$$B_{n,s} = \frac{2\beta_s^2}{\pi R^2 \times (\beta_s^2 - n^2)\{J_n(\beta_s)\}^2} \times \int_0^R \int_{-\pi}^{\pi} u(r,\theta) \times \sin n\theta \times J_n(\beta_s r/R) \times r d\theta dr. \quad (5e)$$

The parameters $\beta_1, \beta_2, \ldots, \beta_s, \ldots$ are the positive roots of $J_n'(\beta) = 0$ with J_n and J_n' the Bessel functions of the nth order and their first derivatives, respectively.

In a FRAP experiment, the fluorescence collected from an area is directly proportional to the amount of the fluorophore present in that area. For an area M defined by a function $m(r,\theta)$, which takes the value 1 inside the area and 0 outside, the amount of fluorophore, $N(t)$, will be given by

$$N(t) = \int_0^R \int_{-\pi}^{\pi} m(r,\theta) \times c(r,\theta,t) \times r d\theta dr. \quad (6)$$

To calculate $N(t)$ with Eqs. 4 and 6, we kept the first five roots ($s = 1$–5) for each of the first 10 Bessel functions ($n = 0$–9). The lowest root value was 1.82 (for $n = 1$ and $s = 1$) and the highest was 27.18 (for $n = 9$ and $s = 5$). The experimental time interval required for bleaching and completing the first scan after bleaching was not negligible, and we have taken it into account by appropriately setting the 0 time in the simulations (see below). The relative fluorescence intensity changes we obtained in this way were representative of the ones measured experimentally. Since the bleaching and measuring areas are not accurately known, we carried out simulations using standardized approximations to the three different bleaching and measuring patterns we employed for the experiments (Fig. 2). We used a fluorophore diffusion coefficient of 2 $\mu m^2\ s^{-1}$ and a disk radius R of 3 μm.

Fig. 2 A shows a representative simulation where the fluorophore has been bleached in the right half of a disk surface. The fluorescence recovery is measured over the same area. This is a simulation of the experimental arrangement of Poo and Cone (25) and of the experiments with BODIPY FL C_{16} using the Argon laser (488-nm line) in a nonconfocal mode (see Fig. 9). Experimentally, it typically took 0.5–1 s from the beginning of bleaching to the end of the first scan, so we set the simulation of the recovery to begin 0.5 s after the end of bleaching. Using Eq. 1, the rate of fluorescence recovery gave a diffusion coefficient of 2.8 $\mu m^2\ s^{-1}$, an overestimation of 40%. Fig. 2 *B* shows a simulation where the fluorophore has been bleached in part of the right half of the disk surface (width of half a disk diameter and a height of 0.3*R*). The fluorescence recovery is measured over two areas, the bleached one and the adjacent one on the left. This is a simulation of experiments with retinol using the Ti:Sapphire IR laser (720 nm) and two-photon excitation (Fig. 3). Again, it took 0.5–1 s from the beginning of bleaching to the end of the first scan in these experiments as well, so the simulation of the recovery begins 0.5 s after the end of bleaching. Using Eq. 1, the rate of fluorescence recovery in the bleached area gave a diffusion coefficient of 4 $\mu m^2\ s^{-1}$, an overestimation of 100%. By contrast, the fluorescence decay in the unbleached adjacent area gave a diffusion coefficient of 2.2 $\mu m^2\ s^{-1}$, an overestimation of only 10%. This difference in the diffusion coefficients obtained from the bleached and unbleached areas was also borne out experimentally (Fig. 3). Finally, Fig. 2 *C* shows a simulation where the fluorophore has been bleached in a strip extending across the disk surface (width of a disk diameter and a height of 0.5*R*). The fluorescence recovery is measured over the bleached area. This is a simulation of experiments with retinol using the Ti:Sapphire IR laser (720 nm) and two-photon excitation (Fig. 4). In these cases, it took 1–2 s from the beginning of bleaching to the end of the first scan, so the simulation of the recovery begins 1 s after the end of bleaching. Using Eq. 1, the rate of fluorescence recovery gave a diffusion coefficient of 3.1 $\mu m^2\ s^{-1}$, an overestimation of 55%.

From the simulations that we carried out, we have concluded that Eq. 1 tends to overestimate the lateral diffusion coefficient. The major factor affecting the extent of overestimation was the size of the bleached area on the disk surface. The symmetry of the bleached area across the horizontal diameter of the disk also played a role: the more symmetric the area, the faster the recovery of fluorescence, leading to higher apparent diffusion coefficient values. The value of the lost fluorescence in a FRAP experiment

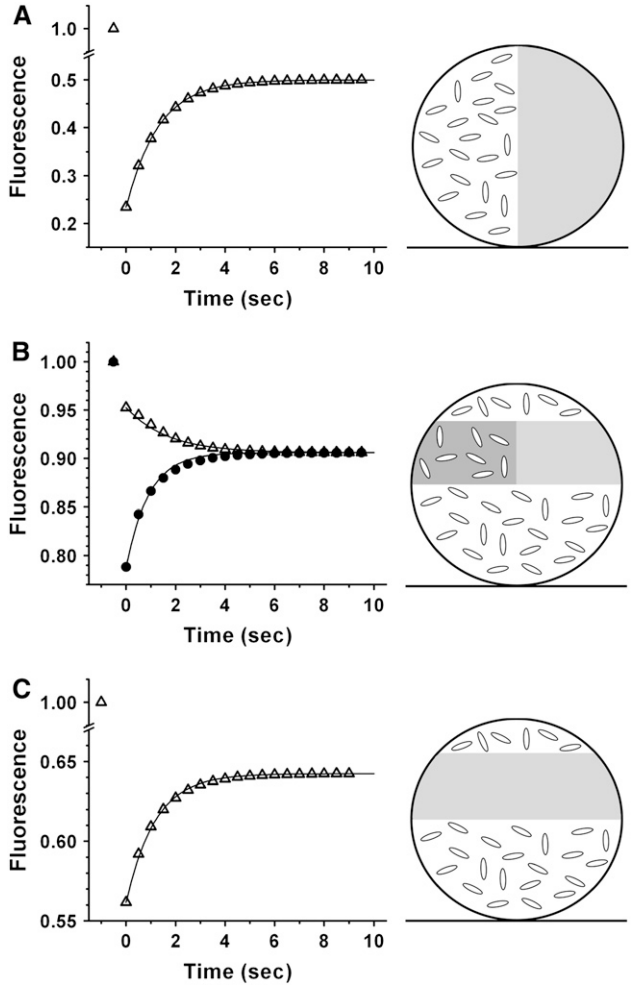

FIGURE 2 Simulations of the different FRAP experiments used for determining lateral diffusion coefficients for a rod outer segment with radius $R = 3$ μm. The fluorophores (oval shapes) are assumed to diffuse in the plane of the disk membrane with coefficient $D = 2$ $\mu m^2\ s^{-1}$. The schemes on the right show transverse cross sections of the outer segment for different bleaching patterns (bleached areas are lightly shaded and are devoid of fluorophore), with the rod lying on the bottom of the chamber and being scanned from the top. The graphs on the left show the corresponding kinetics of fluorescence recovery in bleached or unbleached regions. (*A*) Kinetics of fluorescence recovery after bleaching half of a disk. This pattern models FRAP experiments using single-photon excitation. The line represents a single exponential fit with a rate constant of 0.77 s^{-1}, which, used in conjunction with Eq. 1, would result in an apparent diffusion coefficient of 2.8 $\mu m^2\ s^{-1}$. (*B*) Modeling of FRAP experiments using two-photon excitation and bleaching an area of the right side of the disk. Fluorescence recovered in the bleached disk area (●, *light gray background on right*) faster than in the unbleached (△, *dark gray background on right*). The lines are single exponential fits with rate constants of 1.1 s^{-1} and 0.6 s^{-1} for the bleached and unbleached areas, respectively. Used in conjunction with Eq. 1, these rate constants would result in apparent diffusion coefficients of 4 $\mu m^2\ s^{-1}$ and 2.2 $\mu m^2\ s^{-1}$. (*C*) Modeling of FRAP experiments using two-photon excitation and bleaching a whole strip on the disk. Fluorescence recovered in the bleached disk area with a rate constant of 0.86 s^{-1} (single exponential fit shown by the line), which, used with Eq. 1, would give an apparent diffusion coefficient of 3.1 $\mu m^2\ s^{-1}$.

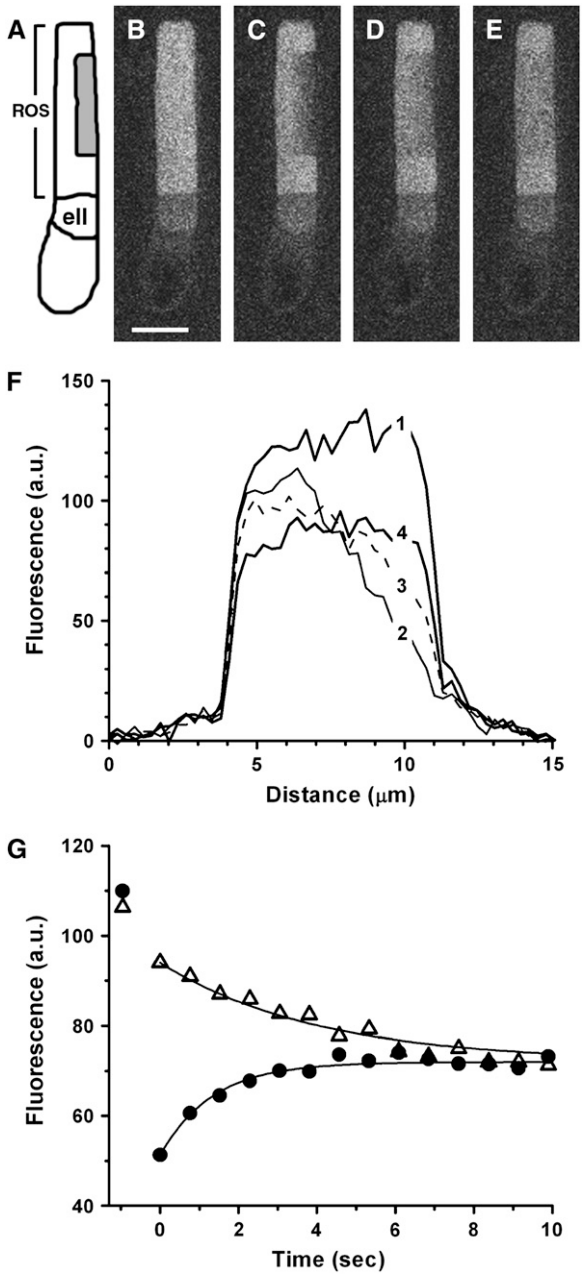

FIGURE 3 Measurement of the mobility of all-*trans* retinol in the disk membranes of an isolated intact frog rod with two-photon FRAP; excitation 720 nm, emission 400–650 nm. In this kind of experiment, simulated in Fig. 2 *B*, a horizontal rectangular area on the right side of the outer segment was bleached. (*A*) Diagram of the cell with bleached area shaded. ROS, rod outer segment; ell, ellipsoid. (*B*) Initial image acquired before retinol bleaching. (*C–E*) Images acquired immediately, and at 2285 and 6092 ms after bleaching, respectively. (*F*) Fluorescence profiles along an outer-segment diameter in the bleached region from images *B* (curve 1), *C* (curve 2), *D* (curve 3), and *E* (curve 4). (*G*) Kinetics of fluorescence recovery in the bleached (●) and unbleached (△) disk areas. The lines represent single exponential fits, with rate constants of 0.75 s^{-1} for the bleached area, and 0.25 s^{-1} for the unbleached area, respectively. The fluorescence recovery in the bleached disk areas is due to retinol movement from the unbleached areas above and below the plane of bleaching, as well as to retinol movement from the areas in the left side. See text for additional details. Images *B–E* are shown at the same intensity scaling. Scale bar is 10 μm.

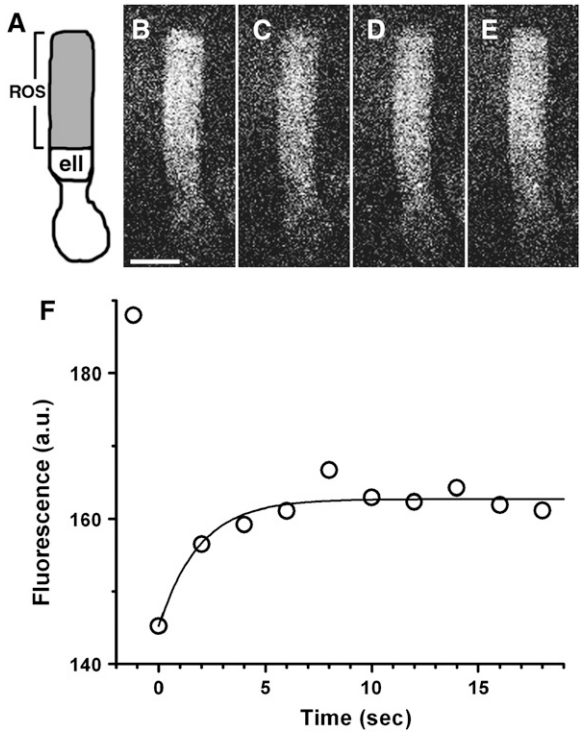

FIGURE 4 Measurement of the mobility of all-*trans* retinol in the disk membranes of an isolated intact frog rod with two-photon FRAP: excitation, 720 nm, emission: 400–650 nm. In this kind of experiment, simulated in Fig. 2 *C*, a horizontal plane spanning the whole outer segment was bleached. (*A*) Diagram of the cell with bleached area shaded: ROS, rod outer segment; ell, ellipsoid. (*B*) Initial image acquired before retinol bleaching. (*C–E*) Images acquired immediately, and at 2 and 14 s after bleaching. (*F*) Kinetics of fluorescence recovery in the bleached area. The line represents a single-exponential fit with a rate constant of 0.53 s^{-1}. The fluorescence recovery is due to retinol movement from the unbleached areas above and below the plane of bleaching. See text for additional details. Images *B–E* are shown at the same intensity scaling. Scale bar, 10 μm.

provides us with an estimate of the size of the bleached area. From these sizes and the simulations, we estimate that in our experiments the use of Eq.1 overestimates the lateral diffusion coefficient by no more than 50–100%. This factor is well within the experimental variability (see Results) and so we have not attempted to correct the estimated diffusion coefficients.

Diffusion on the disk membrane is slowed down by the presence of multiple disk incisures (27) that separate a disk into lobes. Poo and Cone (25) estimated that the presence of the incisures slowed down diffusion by a factor of 2.7. We have not corrected the apparent lateral diffusion coefficient values for this effect. However, we have taken this effect into account to estimate the value of the diffusion coefficient of retinol in the plasma membrane of the rod outer segment (see Discussion).

Analysis of longitudinal diffusion

For longitudinal diffusion of the fluorophores along the length of the outer segment, the fluorophore was bleached in one-half of the outer segment (proximal or distal) and the fluorescence recovery was analyzed to obtain the diffusion coefficient for longitudinal mobility. Assuming that there is no significant fluorophore loss from the outer segment during the course of the experiment, the equilibration of the fluorophore along the length of the outer segment can be described by the diffusion equation for a rod insulated at

both ends (26 (see p. 101, Eq. 6)). The initial condition of the experiment was set by bleaching the fluorophore in one half of the outer segment, in which case the equation becomes

$$F(x,t) = F_2 + \Delta F \times \left(\frac{1}{2} + \frac{2}{\pi} \cdot \sum_{m=0}^{\infty} \frac{(-1)^m}{2m+1} \times e^{-(2m+1)^2 \alpha t} \times \cos\frac{(2m+1)\pi x}{L}\right), \quad (7)$$

where L is the outer-segment length, $F(x,t)$the outer-segment fluorescence at position x along the length and at time t after the bleach, F_1 and F_2 the initial values of outer-segment fluorescence in the unbleached and bleached half, respectively, with $\Delta F = F_1 - F_2$, and

$$\alpha = \pi^2 \times \frac{D_{axial}}{L^2}, \quad (8)$$

where D_{axial} is the apparent diffusion coefficient for movement along the length of the outer segment. To avoid significant loss of the fluorophore from the outer segment, it was necessary to limit the experiments to relatively short periods of time, 30–45 min at the most. At this timescale, equilibration was reached only for the cells with the shorter outer segments, in which case the recovery of fluorescence could be approximated with a single exponential (the first term of the infinite sum in Eq. 7), giving the parameter α of Eqs. 7 and 8 as the rate of recovery, which together with the outer-segment length was used to obtain D_{axial}. For longer outer segments, the parameter α was obtained from the slope of the fluorescence profile at the middle of the outer segment at different time points after the bleach (for a related older method, see Crank (28), p. 232, Fig. 10.2):

$$\left.\frac{\partial F}{\partial x}(x,t)\right|_{x=L/2} = -\frac{2 \times \Delta F}{L} \times \sum_{m=0}^{\infty} e^{-(2m+1)^2 \alpha t}. \quad (9)$$

RESULTS

The lateral mobility of retinol on the disk membrane was measured by bleaching the fluorophore in an area of the disk and following the equilibration of fluorescence as unbleached retinol moved into the bleached area. Fig. 3 *B* shows the two-photon fluorescence image of an intact frog rod photoreceptor, ~50 min after a light exposure that photoisomerized the full complement of outer-segment chromophore in rhodopsin. Most of the endogenous retinoid has been converted to retinol, which is responsible for the outer-segment fluorescence. The average outer-segment concentration of retinol would then be similar to that of rhodopsin, ~2.5 mmol/L (23), and, as its aqueous solubility is very low, ~100 nmol/L (7), it will essentially be confined to the disk membranes. Retinol was bleached in a volume of the outer segment by exposure to a higher laser intensity (Fig. 3 *C*). The bleached volume does not extend throughout the width of the outer segment, as the span of excitation, ~2 μm, is only a fraction of the outer-segment diameter, ~6 μm, as pointed out in the previous section. Disks are perpendicular to the plane of the image, so at the level of a disk membrane within the bleached volume, retinol has been destroyed in a strip that extends over half a disk diameter and is ~2 μm wide. With time, fluorescence recovers in the bleached strip (Fig. 3, *D* and *E*), as retinol moves in from the areas above and below, as well as from the left, unbleached half of the disk. The fluorescence in the bleached region cannot recover to its original value, as a significant amount of retinol has been bleached. Fig. 3 *F* shows the retinol fluorescence intensity profiles along an outer-segment diameter at different times after bleaching. Fluorescence increases in the bleached half-diameter and decreases in the unbleached half; Fig. 3 *G* plots the respective intensity changes as a function of time. The intensity values at the bleached and unbleached halves reach the same value, reflecting the attainment of equilibrium and the absence of a significant amount of immobile retinol. Retinol moves into the bleached strip from the unbleached disk areas above and below, as well as from the unbleached half-disk on the left, and the exponential fit gives a rate of fluorescence recovery $k = 0.75\ s^{-1}$. The diameter of the outer segment for this cell was $d = 7.2\ \mu m$, which, using Eq. 1, gave a lateral diffusion coefficient $D = 3.9\ \mu m^2\ s^{-1}$. Retinol also moves out of the unbleached strip on the left as it equilibrates over the whole disk and thus the fluorescence decays in the unbleached half. That rate of decay is $k = 0.25\ s^{-1}$, giving a lateral diffusion coefficient $D = 1.3\ \mu m^2\ s^{-1}$. This difference between the diffusion coefficients measured from the fluorescence rates of recovery in the bleached and unbleached halves was consistent across cells, in agreement with model simulations (Fig. 2 *B*). The diffusion coefficients obtained from the bleached and unbleached halves of $n = 7$ cells were $4.4 \pm 0.8\ \mu m^2\ s^{-1}$ (range 2–8 $\mu m^2\ s^{-1}$) and $2.1 \pm 0.5\ \mu m^2\ s^{-1}$ (range 0.6–4.9 $\mu m^2\ s^{-1}$), respectively. The kinetics of fluorescence recovery in the bleached half include a significant contribution from the close-by areas above and below, that is, over a smaller area, resulting in apparently faster kinetics with a correspondingly higher diffusion coefficient. As demonstrated by model simulations, the kinetics of fluorescence decay in the unbleached strip reflect more closely the equilibration process after bleaching, and so we have taken the corresponding diffusion coefficient of 2.1 $\mu m^2\ s^{-1}$ as the one representing the mobility of retinol on the disk membrane.

Fig. 4 *B* is the initial fluorescence image of an intact rod for which retinol was bleached in a slab spanning the whole outer segment (see Fig. 2 *C* for a model simulation). Fig. 4 *C* shows the image acquired immediately after bleaching. With time, as retinol moves in from the areas above and below, fluorescence recovers in the bleached area (Fig. 4, *D* and *E*). The rate of recovery (Fig. 4 *F*) for the whole bleached area was $0.53\ s^{-1}$, and with an outer-segment diameter $d = 7.2$ μm, gave a lateral diffusion coefficient $D = 2.8\ \mu m^2\ s^{-1}$. From a total of $n = 20$ cells, we have obtained an overall rod outer-segment lateral diffusion coefficient of $2.5 \pm 0.3\ \mu m^2\ s^{-1}$ (range 0.9–5.9 $\mu m^2\ s^{-1}$). This value is consistent with the estimate of 2.1 $\mu m^2\ s^{-1}$ obtained from the monitoring of the movement of retinol out of unbleached disk areas (see above).

The lateral mobility of retinol did not depend significantly on the position of the disk along the length of the rod outer segment. For $n = 13$ cells, there was enough resolution to allow the measurement of fluorescence recovery in different

parts of the outer segment. We separated the outer segment into three areas of equal length, each comprising one-third of the outer segment, top, middle, and base. The lateral diffusion coefficients for top, middle, and base were 2.2 ± 0.5, 2.5 ± 0.4, and 2.5 ± 0.4 $\mu m^2\ s^{-1}$, respectively. Although it appeared that the diffusion coefficient for retinol in the top third of the outer segment disks is smaller than in the middle and the base, the difference is not statistically significant.

The value for the diffusion coefficient of retinol in the disk membrane is for retinol that has been formed from the 11-*cis* retinal originally bound in the visual pigment. Cellular regulation of the movement of retinol in the rod outer segment could manifest itself as a constraint on the mobility of endogenously produced retinol. Although the value obtained for the lateral diffusion coefficient is consistent with unrestricted diffusion (see Discussion), we have further probed the possibility of a special association of the endogenously produced retinol with outer-segment components by measuring the mobility of exogenously added retinol. The use of exogenous retinol also allows the mobility measurements in ROS, which do not have the metabolic competence to generate endogenous retinol. For these experiments, endogenous retinol was removed with BSA, and exogenous all-*trans* retinol was added to concentrations similar to those of the endogenous. The average lateral diffusion coefficient for exogenous retinol in isolated ROS was 3.2 ± 0.4 $\mu m^2\ s^{-1}$ ($n = 10$; range 1.7–5.5 $\mu m^2\ s^{-1}$) and was virtually identical to that obtained from the outer segments of intact cells and ROS-RIS, 3.2 ± 0.5 $\mu m^2\ s^{-1}$ ($n = 7$; range 1.7–5.3 $\mu m^2\ s^{-1}$). We also carried out experiments with high loads of exogenous all-*trans* retinol, 5–10 times the endogenous levels, and obtained significantly lower lateral diffusion coefficients: 1.1 ± 0.1 $\mu m^2\ s^{-1}$ ($n = 8$) in isolated ROS, and 1.1 ± 0.2 $\mu m^2\ s^{-1}$ ($n = 9$) in the outer segments of intact cells and ROS-RIS.

After characterizing the movement of all-*trans* retinol in the plane of the disk membrane, we examined its mobility along the outer-segment axis. Although retinol did move along the length of the outer segment, its movement was very slow, making it difficult to obtain the full time course of the fluorescence recovery kinetics, as it took a long time to reach equilibration. Retinol does have a small aqueous solubility, so as time passes after retinol formation, it slowly leaves the outer segment (8,29) and goes into the bulk solution, complicating the analysis of mobility measurements. For cells with relatively short outer segments (length <20 μm), it was possible to reach equilibration within such a time frame that retinol loss was not significant (8,20) and the diffusion model associated with Eq. 7 was applicable. Fig. 5 shows the measurement of the axial mobility of retinol in a rod outer segment that had a length $L = 13\ \mu m$. Fig. 5 *B* is the initial fluorescence image before bleaching; Fig. 5, *C–E*, shows the images immediately and at 180 and 420 s after bleaching. There is a slow equilibration of retinol along the length of the outer segment, with a rate of $4.6 \times 10^{-3}\ s^{-1}$ (Fig. 5 *F*), which, using Eq. 8, gives an axial diffusion coefficient of 0.081 $\mu m^2\ s^{-1}$. The axial mobility of retinol was evident in longer outer segments as well. However, the equilibration of retinol along the length of the outer segment in these cases took a very long time, and it was not possible to analyze the recovery kinetics with a rising exponential. Instead, the gradient of retinol concentration across the bleaching boundary was used to obtain an estimate of the rate of recovery. Fig. 6 shows such an experiment in a cell with an outer segment of length $L = 57\ \mu m$. Fig. 6 *B* is the initial fluorescence image, whereas Fig. 6, *C* and *D*, shows the images immediately after and 1440 s after bleaching, respectively. Fig. 6 *E* shows the fluorescence intensity profiles along the axis of the outer segment from Fig. 6, *B* and *C*. The fairly sharp-intensity boundary between the bleached and unbleached areas corresponds to $x = 0$. Fig. 6 *F* shows the intensity profile from Fig. 6 *D*, 1440 s after bleaching. There is clear movement of retinol across the bleaching boundary with time. The slope at the boundary 1440 s after bleaching was $\partial F/\partial x = -2.4\ \mu m^{-1}$, the initial

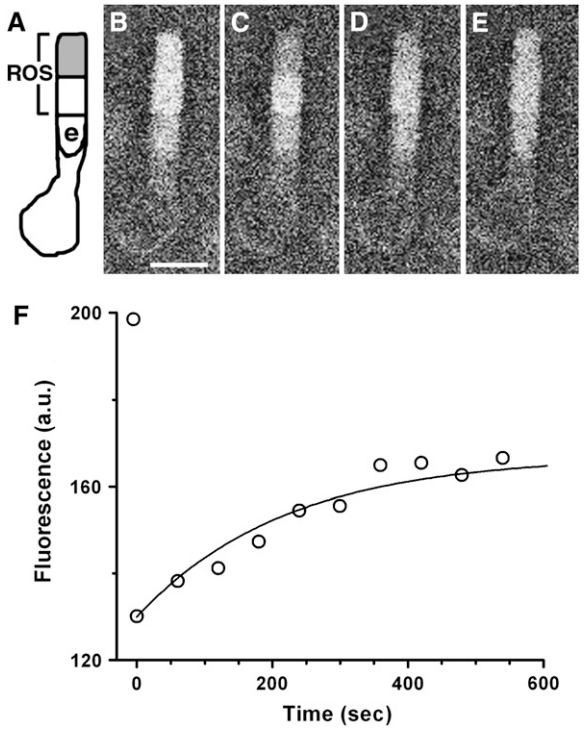

FIGURE 5 Measurement of the mobility of all-*trans* retinol along the length of an isolated intact frog rod with two-photon FRAP: excitation 720 nm, emission 400–650 nm. (*A*) Diagram of the cell with bleached area shaded. ROS, rod outer segment; e, ellipsoid. (*B*) Initial image acquired before retinol bleaching. (*C–E*) Images acquired immediately, and at 180 and 420 s after bleaching. (*F*) Kinetics of fluorescence recovery in the bleached volume. The line represents a single-exponential fit, with a rate constant of $4.6 \times 10^{-3}\ s^{-1}$, giving an apparent axial diffusion coefficient of 0.081 $\mu m^2\ s^{-1}$. Images *B–E* are shown at the same intensity scaling. Scale bar, 10 μm.

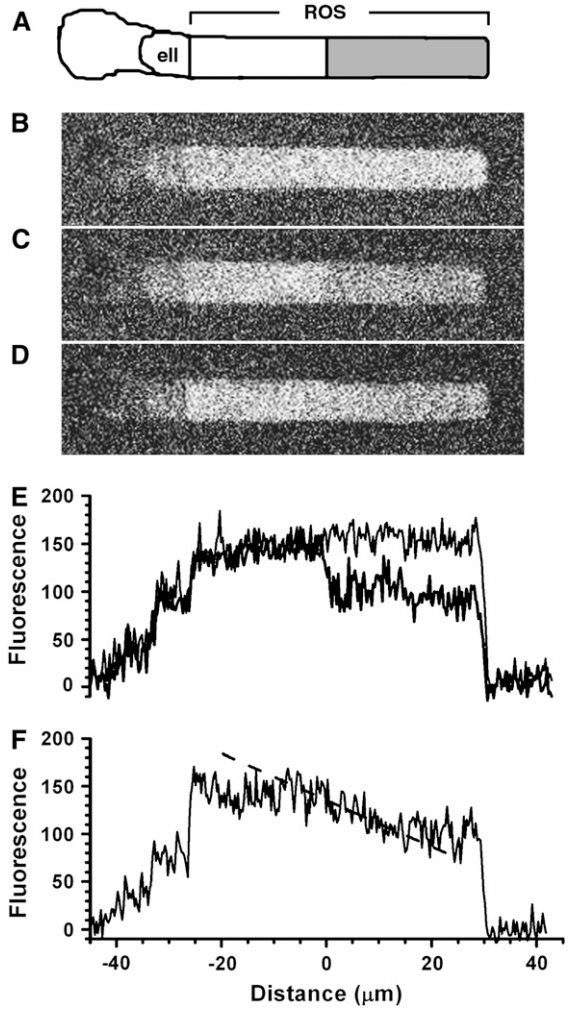

FIGURE 6 Measurement of the mobility of all-*trans* retinol along the length of an isolated intact frog rod with two-photon FRAP: excitation 720 nm, emission 400–650 nm. (*A*) Diagram of the cell with bleached area shaded. ROS, rod outer segment; ell, ellipsoid. (*B*) Initial image acquired before retinol bleaching, (*C–D*) Images acquired immediately and at 1440 s after bleaching. (*E*) Fluorescence intensity profiles before (*thin line*) and immediately after (*thick line*) bleaching. (*F*) Fluorescence intensity profile 1440 s after bleaching; the straight dashed line represents the slope of the intensity profile at the boundary between bleached and unbleached regions. The slope of the intensity profile gave a rate constant for movement of 6.9×10^{-5} s^{-1}, resulting in an apparent axial diffusion coefficient of 0.023 μm^2 s^{-1}. Images *B–D* are shown at the same intensity scaling. The fluorescence intensity profiles are aligned with the images.

values of outer-segment fluorescence in the unbleached and bleached halves were $F_1 = 194$ and $F_2 = 144$, respectively, with $\Delta F = F_1 - F_2 = 50$. Eq. 9 then gives for the rate of axial movement of retinol a value $\alpha = 6.9 \times 10^{-5}$ s^{-1}, resulting in an apparent axial diffusion coefficient of 0.023 μm^2 s^{-1} (using Eq. 8 with $L = 57$ μm). The average apparent axial diffusion coefficient from $n = 14$ cells was 0.07 ± 0.01 μm^2 s^{-1} (range 0.016–0.150 μm^2 s^{-1}). Exogenous retinol, loaded at concentrations similar to the endogenous, moved along the length of rod outer segments with virtually the same diffusion coefficient. Fig. 7 shows an experiment with exogenous retinol, similar to the one presented for endogenous retinol in Fig. 5. The axial diffusion coefficient measured from this cell was 0.036 μm^2 s^{-1}, and from $n = 6$ cells, the average value was 0.05 ± 0.01 μm^2 s^{-1} (range 0.014–0.098 μm^2 s^{-1}).

The observed axial movement of both endogenous and exogenous retinol was consistent with passive diffusion, as the rate of movement, measured either from overall recovery kinetics (as in Figs. 5 and 7) or from the rate of spilling over the concentration boundary (as in Fig. 6), scaled with the inverse square of the rod outer-segment length (Fig. 8), as expected from Eq. 8. The straight line shown in the figure has been drawn with a slope corresponding to the average diffusion coefficient of 0.07 μm^2 s^{-1}. A linear least-squares fit of the data in Fig. 8 gives a value of 0.09 μm^2 s^{-1} (not shown).

The values for the lateral and axial diffusion coefficients that describe the mobility of retinol in the outer segment are consistent with passive, unrestricted diffusion (see Discussion). We tested this notion directly by comparing the

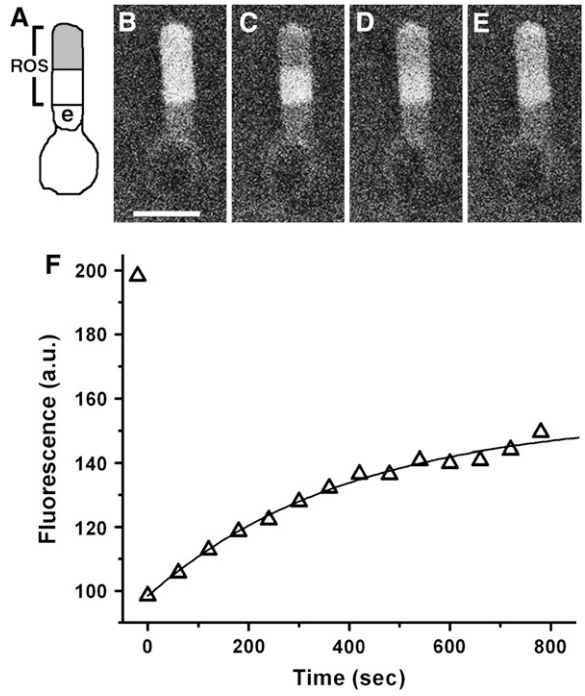

FIGURE 7 Measurement of the mobility of exogenously added all-*trans* retinol along the length of an isolated intact frog rod with two-photon FRAP: excitation 720 nm, emission 400–650 nm. The endogenously generated retinol was removed by BSA, and exogenous retinol was added to a level similar to that reached by the endogenous. (*A*) Diagram of the cell with bleached area shaded. ROS, rod outer segment; e, ellipsoid. (*B*) Initial image acquired before retinol bleaching. (*C–E*) Images acquired immediately, and at 300 and 780 s after bleaching. (*F*) Kinetics of fluorescence recovery in the bleached volume. The line represents a single exponential fit, with a rate constant of 2.5×10^{-3} s^{-1}, giving an apparent axial diffusion coefficient of 0.036 μm^2 s^{-1}. Images *B–E* are shown at the same intensity scaling. Scale bar, 10 μm.

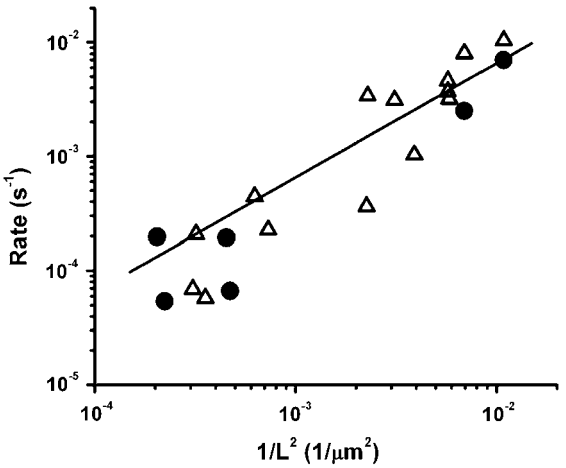

FIGURE 8 The mobility rate constants for the movement of endogenous (△) and exogenous (●) retinol along the length of the rod outer segment scale linearly with the inverse square of outer-segment length, consistent with passive diffusion. The straight line passes through the origin and corresponds to the average value of 0.07 $\mu m^2\ s^{-1}$ for the axial diffusion coefficient. The data have been plotted on a log-log plot for clarity.

diffusion in rod outer segments of a fluorescent-labeled fatty acid, BODIPY FL C_{16}, which, like retinol, consists of a single, elongated hydrophobic module. Fig. 9 presents an experiment measuring the lateral mobility of BODIPY FL C_{16}. Fig. 9 *A* shows the single-photon nonconfocal fluorescence image of a frog ROS-RIS loaded with the fluorophore. With these imaging settings, the collected fluorescence comes from the probe throughout the thickness of the outer segment. The probe in the left half of the outer segment was bleached (Fig. 9 *B*) with a higher laser intensity, and, with time, as the probe redistributed, the fluorescence in the bleached area recovered (Fig. 9, *C* and *D*). A model simulation for this kind of experiment is shown in Fig. 2 *A*. The lateral diffusion coefficient measured from this cell was 1.4 $\mu m^2\ s^{-1}$, and from $n = 15$ cells the average value was 2.2 ± 0.2 $\mu m^2\ s^{-1}$ (range 1.4–3.9 $\mu m^2\ s^{-1}$), in close agreement with the value obtained for retinol. BODIPY FL C_{16} moved along the length of the outer segment as well, with an axial diffusion coefficient of 0.04 ± 0.01 $\mu m^2\ s^{-1}$ ($n = 7$, range 0.020–0.056 $\mu m^2\ s^{-1}$), similar to the one obtained for retinol. Therefore, the diffusion of retinol is similar to that of the fatty acid analog, as expected for passive, unrestricted diffusion. Table 1 summarizes the different diffusion coefficient measurements for retinol as well as for BODIPY FL C_{16}.

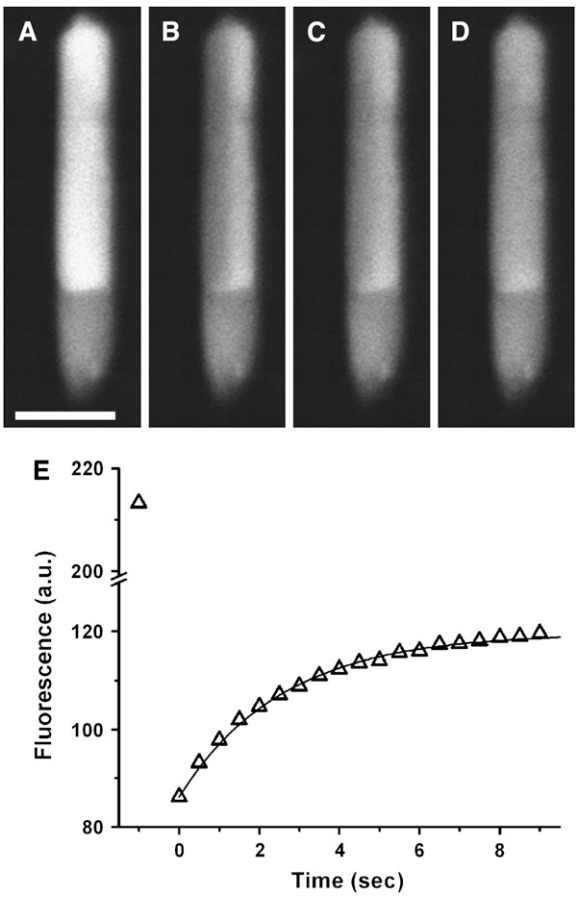

FIGURE 9 Measurement of the mobility of BODIPY FL C_{16} in the disk membranes of an isolated frog ROS-RIS with single-photon FRAP: excitation 488 nm, emission 505–700 nm. In this kind of experiment, simulated in Fig. 2 *A*, the whole left half of a disk was bleached. (*A*) Initial image acquired before dye bleaching. (*B–D*) Images acquired immediately, and at 1 and 9 s after bleaching. (*E*) Kinetics of fluorescence recovery. The line represents a single exponential fit, with rate constant of 0.39 s^{-1}, giving a value of 1.4 $\mu m^2\ s^{-1}$ for the lateral diffusion coefficient. Images *A–D* are shown at the same intensity scaling. Scale bar, 10 μm.

DISCUSSION

All-*trans* retinol is one of the key intermediates of the visual cycle, as it is the last intermediate in the portion of the cycle that takes place in the rod photoreceptor outer segments.

In current models of the cycle, the precursors of retinol in the outer segment are either bound covalently in the visual pigment site (in the form of the 11-*cis* and all-*trans* retinyl moieties), sequestered inside the disks in the form of a Schiff base complex with phosphatidylethanolamine (6), or, in the case of free all-*trans* retinal, reduced to all-*trans* retinol through an energy-dependent process (4,5). All-*trans* retinol is thought to be removed from the rod outer segment through specialized carrier proteins to be transported to the retinal pigment epithelial cells for subsequent processing (10,11). In contrast to these other intermediates and steps, our results indicate that in rod photoreceptor outer segments the bulk of all-*trans* retinol itself diffuses passively and unrestricted and does not appear to be significantly sequestered or bound to carrier proteins.

In examining potential pitfalls to this conclusion, an important concern is whether the observed fluorescence recoveries in the FRAP experiments are due to the regeneration of retinol through chemical reactions instead of

TABLE 1 Summary of the apparent diffusion coefficients measured

	Retinol, endogenous	Retinol, exogenous	BODIPY FL C_{16}
Intact, lateral	2.5 ± 0.3 (20)	3.2 ± 0.5 (7)	2.2 ± 0.2 (15)
ROS, lateral	ND	3.2 ± 0.4 (10)	ND
Intact, axial	0.07 ± 0.01 (14)	0.05 ± 0.01 (6)	0.04 ± 0.01 (7)

Values are represented as mean ± SE, units are $\mu m^2\ s^{-1}$, and the number of cells used is given in parentheses. ''Lateral'' refers to the diffusion coefficient in the disk membrane. For lateral mobility measurements, data from ROS-RIS fragments are included together with those from intact cells. For axial mobility measurements the data are exclusively from intact cells. The only diffusion coefficient measured in broken-off rod outer segments, ROS, was for exogenous all-*trans* retinol moving in the plane of the disk membrane. ND, not determined.

movement. This was highly unlikely because, as mentioned in Methods, under the conditions of the experiment, most of the retinoid is in the form of retinol to begin with. In addition, fluorescence recovery consisted of a fluorescence increase in the bleached areas, but a decrease in the unbleached ones (Fig. 3), consistent with the movement of retinol from the latter to the former. Finally, the 100- to 10,000-times difference in the fluorescence recovery rates between the lateral and axial FRAP types of measurements, and the scaling of the fluorescence recovery rate with the inverse square of rod outer-segment length (Fig. 8) strongly argue against any significant contribution to the measured rates by a chemical reaction.

The value we obtained for the diffusion coefficient of all-*trans* retinol in the disk membrane, 2.5 $\mu m^2\ s^{-1}$, is similar to that for the diffusion of lipids in biological membranes, 2–4 $\mu m^2\ s^{-1}$ (30). It is also similar to that obtained for fluorescent-labeled phosphatidylcholine and phosphatidylethanolamine in salamander rod outer segments, 4–5 $\mu m^2\ s^{-1}$ (31). No significant fraction of retinol appears to be immobilized, as its concentration equilibrates between bleached and unbleached areas (Fig. 3). The additional observation that the diffusion coefficients of exogenous retinol and of a fatty acid probe, BODIPY FL C_{16}, are also the same, is consistent and indicates that all-*trans* retinol diffuses unrestricted in the plane of the disk membrane. The lower diffusion coefficient, 1.1 ± 0.2 $\mu m^2\ s^{-1}$, obtained for high concentrations of exogenously added retinol, is probably due to crowding. As there are ~75 lipids per rhodopsin (see calculations in Daemen (32)), exogenous retinol at 5–10 times the concentration of the endogenous would reach almost 13% of the molar concentration of the membrane lipids. For rhodopsin, reducing its concentration in the disk membrane results in a higher lateral diffusion coefficient due to less crowding (33).

The results do not exclude the possibility that a small fraction of retinol is bound to a carrier protein. At the concentrations of retinol present during the course of these experiments, the only protein in sufficiently high concentrations to act as a carrier would be rhodopsin, more precisely, the apoprotein opsin. Retinol could bind transiently to a secondary retinoid binding site on opsin (34,35). The diffusion coefficient of rhodopsin has been measured to be in the order of 0.4–0.5 $\mu m^2\ s^{-1}$ (25,36), and a virtually identical value is obtained for fluorescently labeled rhodopsin when measured in the same way as BODIPY FL C_{16} (31). Since rhodopsin moves several times more slowly than what we measure for retinol, any binding of retinol to rhodopsin would be relatively weak so that it would reduce the mobility slightly, but not drastically.

The mobility of retinol in the disk membrane is significantly slowed down by the presence of multiple incisures that separate the disk surface into lobes (27). Poo and Cone (25) estimated that the presence of the incisures slowed down diffusion by a factor of 2.7. Therefore, the diffusion coefficient in the absence of incisures would be $2.7 \times 2.5\ \mu m^2\ s^{-1} \approx 6.8\ \mu m^2\ s^{-1}$, a value that should reflect more closely the intrinsic viscosity of the membrane.

The axial diffusion of retinol has been investigated before. An initial report (17) failed to observe redistribution of the endogenous retinol produced after localized partial bleaches of rhodopsin. A subsequent study, however (18), concluded that at least a portion of the retinol can move axially along the length of the outer segment. These older experiments were hampered by having to look at mobility by producing retinol locally. After the initial localized generation of retinol, the measuring light would produce retinol throughout the outer segment, thereby allowing only one meaningful measurement per cell. As a result, the profiles of the retinol distribution at different times after bleaching were obtained from different outer segments, permitting only broad qualitative inferences. Azuma et al. (19) used microspectrophotometry, and, in the face of similar limitations, also concluded that retinol could move axially. The experiments described here have established that retinol indeed moves along the length of the outer segment, with an apparent diffusion coefficient of 0.07 ± 0.01 $\mu m^2\ s^{-1}$, virtually the same as the one measured for exogenous retinol. As the rate for the process of retinol equidistribution scales with the inverse square of the length of the outer segment (Fig. 8), the process is consistent with passive diffusion and as such does not require energy input. This is further corroborated by the similar value of 0.04 ± 0.01 $\mu m^2\ s^{-1}$ obtained for the diffusion coefficient for the axial movement of BODIPY FL C_{16}.

The axial mobility of retinol suggests that there is significant amount of retinol present in axially mobile pools. These mobile pools should account for the observed value of the axial diffusion coefficient. Since the lateral diffusion coefficient measurements have suggested that retinol diffuses unrestricted, there are only three retinol pools to consider: disk membranes, plasma membrane, and aqueous cytoplasm (Fig. 10). In terms of axial diffusion, the retinol on the disks is immobile, so axial mobility has to rely on the aqueous and plasma membrane pools. Since the aqueous solubility of retinol is very low, virtually all of the retinol will

be in the disk and plasma membranes. The repeat distance between the disks, δ, is ~30 nm (37), so for an outer-segment diameter $d = 6\ \mu$m, the plasma membrane area is $\pi\delta d/2\pi(d/2)^2 = 1\%$ of the disk membrane. As a result, 99% of the retinol will be in the disk membranes, and 1% on the plasma membrane. Since the concentration of retinol in the rod outer segment is expected to be similar to that of rhodopsin, ~2.5 mmol/L (23), and the aqueous solubility of retinol is ~100 nmol/L (7), the fraction of retinol in the cytoplasm will be $\sim 4 \times 10^{-5}$ (100 nmol/2.5 mmol).

The plasma membrane and disk pools of retinol are expected to be in rapid equilibrium, as retinol is readily removed from the rod outer segment upon exposure to lipophilic carriers (8,29). In addition, membrane tracers loaded from the extracellular side of the plasma membrane swiftly label the disk membranes as well (31). For simplicity, we can also assume that the minute aqueous pool of retinol is also in rapid equilibrium with the disk and plasma membrane pools. Thus, with the three pools of retinol being at rapid equilibrium, the axial diffusion coefficient will be given by

$$D_{\text{axial}} = f_{\text{aq}} \times D_{\text{aq}} + f_{\text{PM}} \times D_{\text{PM}}, \tag{10}$$

where D_{aq} is the diffusion coefficient of retinol in the cytoplasm, D_{PM} the diffusion coefficient of retinol on the plasma membrane, and f_{aq} and f_{PM} the fractions of retinol in the axially mobile pools of the cytoplasm and plasma membrane. Eq. 10 is based on Eq. 27 of Zhou and Neher (38), derived for Ca^{2+} diffusion, and is a generalization of the textbook approach (see Eq. 14.3 of Crank (28)) for diffusion with binding; it follows directly from Fick's law (see Eq. 20 of Zhou and Neher (38)). Since the plasma membrane contains no incisures, $D_{\text{PM}} = 6.8\ \mu\text{m}^2\ \text{s}^{-1}$ (see above), whereas $D_{\text{aq}} = 300\ \mu\text{m}^2\ \text{s}^{-1}$ (39). Also, $f_{\text{PM}} = 0.01$ and $f_{\text{aq}} = 4 \times 10^{-5}$ (see above). After substituting the values into Eq. 10, we obtain $D_{\text{axial}} = 0.08\ \mu\text{m}^2\ \text{s}^{-1}$, in excellent agreement with the experimentally determined value. This analysis also shows that the plasma membrane provides the conduit that is primarily responsible for the axial mobility of retinol. The contribution of the cytoplasmic pool of retinol is minor, ~15%, because although the mobility of retinol in that pool is high, the size of the pool is too small. The similar diffusion coefficient measured for the axial mobility of BODIPY Fl C_{16}, $0.04\ \mu\text{m}^2\ \text{s}^{-1}$, is consistent with the nonspecific conduit provided by the plasma membrane. In conclusion, the bulk of the all-*trans* retinol produced in rod photoreceptor outer segments from the bleaching of rhodopsin moves unrestricted and is not tightly bound to any carrier proteins. Its axial mobility along the length of the rod outer segment can be quantitatively accounted for by diffusion in the plasma membrane and the rapid equilibration between the disk and plasma membrane retinol pools.

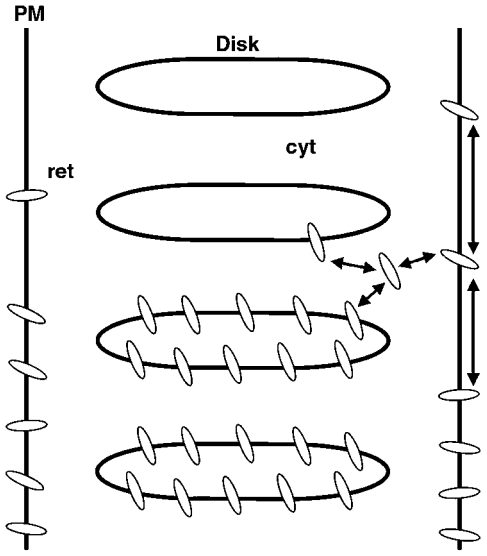

FIGURE 10 Schematic diagram illustrating the distribution of retinol and its axial diffusion conduits in rod outer segments. PM, plasma membrane; ret, retinol; cyt, cytoplasmic space. The diagram represents the situation in a FRAP experiment in which retinol has been bleached in the upper half of the outer segment. The diagram is not drawn to scale; the disk diameter is ~6 μm, and the distance between disks is 15 nm; the distance between the disk rim and the plasma membrane is also ~15 nm. The rod outer segment contains ~1000 disks. Because of low solubility, very small amounts of retinol are free in the cytoplasm; ~99% of the retinol is in the disk membranes and ~1% in the plasma membrane. Retinol equilibrates rapidly between the disk and plasma membranes, allowing substantial axial mobility through the plasma membrane.

The finding that there is no specialized processing for retinol contrasts dramatically with the energy-dependent processing of its precursor, all-*trans* retinal, upon its release from photoactivated rhodopsin. In that case, active transport by ABCR (6) and enzymatic reduction requiring NADPH (4,5) are important steps in the handling of all-*trans* retinal by the cell machinery. A possible functional reason for the difference may be the need to rapidly eliminate all-*trans* retinal, which is a reactive aldehyde and can also act as a photosensitizer (40,41), as its absorption spectrum ($\lambda_{\text{max}} \sim$ 380 nm) extends into the visible range. All-*trans* retinol is much less toxic, and its phototoxicity is unlikely to be a problem, as its spectrum is shifted to the blue ($\lambda_{\text{max}} \sim$ 325 nm) and away from the visible range; thus, no distinct processing is necessary. The low aqueous solubility of all-*trans* retinol, on the other hand, may require the presence of specialized lipophilic carriers like interphotoreceptor retinoid binding protein for its removal from the rod outer-segment membranes and its transport to the pigment epithelial cells for further processing.

We thank Drs. Masahiro Kono and Rosalie K. Crouch for helpful discussions and comments on the manuscript.

This research was supported by National Institutes of Health/National Eye Institute grants EY14850 (Y.K.), EY14793, and an unrestricted grant to Medical University of South Carolina Storm Eye Institute from Research to Prevent Blindness, Inc., New York, NY. The Zeiss LSM 510 Non-Linear Optical Confocal Microscope is part of a core facility at the Medical University of South Carolina (supported by 1S10RR015776).

REFERENCES

1. Lamb, T. D., and E. N. Pugh, Jr. 2004. Dark adaptation and the retinoid cycle of vision. *Prog. Retin. Eye Res.* 23:307–380.
2. McBee, J. K., K. Palczewski, W. Baehr, and D. R. Pepperberg. 2001. Confronting complexity: the interlink of phototransduction and retinoid metabolism in the vertebrate retina. *Prog. Retin. Eye Res.* 20:469–529.
3. Saari, J. C. 2000. Biochemistry of visual pigment regeneration: the Friedenwald lecture. *Invest. Ophthalmol. Vis. Sci.* 41: 337–348.
4. Futterman, S., A. Hendrickson, P. E. Bishop, M. H. Rollins, and E. Vacano. 1970. Metabolism of glucose and reduction of retinaldehyde in retinal photoreceptors. *J. Neurochem.* 17:149–156.
5. Palczewski, K., S. Jager, J. Buczylko, R. K. Crouch, D. L. Bredberg, K. P. Hofmann, M. A. Asson-Batres, and J. C. Saari. 1994. Rod outer segment retinol dehydrogenase: substrate specificity and role in phototransduction. *Biochemistry.* 33:13741–13750.
6. Weng, J., N. L. Mata, S. M. Azarian, R. T. Tzekov, D. G. Birch, and G. H. Travis. 1999. Insights into the function of Rim protein in photoreceptors and etiology of Stargardt's disease from the phenotype in abcr knockout mice. *Cell.* 98:13–23.
7. Szuts, E. Z., and F. I. Harosi. 1991. Solubility of retinoids in water. *Arch. Biochem. Biophys.* 287:297–304.
8. Tsina, E., C. Chen, Y. Koutalos, P. Ala-Laurila, M. Tsacopoulos, B. Wiggert, R. K. Crouch, and M. C. Cornwall. 2004. Physiological and microfluorometric studies of reduction and clearance of retinal in bleached rod photoreceptors. *J. Gen. Physiol.* 124:429–443.
9. Kamp, F., D. Zakim, F. Zhang, N. Noy, and J. A. Hamilton. 1995. Fatty acid flip-flop in phospholipid bilayers is extremely fast. *Biochemistry.* 34:11928–11937.
10. Okajima, T. I., D. R. Pepperberg, H. Ripps, B. Wiggert, and G. J. Chader. 1989. Interphotoreceptor retinoid-binding protein: role in delivery of retinol to the pigment epithelium. *Exp. Eye Res.* 49: 629–644.
11. Adler, A. J., and R. B. Edwards. 2000. Human interphotoreceptor matrix contains serum albumin and retinol-binding protein. *Exp. Eye Res.* 70:227–234.
12. Ripps, H., N. S. Peachey, X. Xu, S. E. Nozell, S. B. Smith, and G. I. Liou. 2000. The rhodopsin cycle is preserved in IRBP ''knockout'' mice despite abnormalities in retinal structure and function. *Vis. Neurosci.* 17:97–105.
13. Palczewski, K., J. P. Van Hooser, G. G. Garwin, J. Chen, G. I. Liou, and J. C. Saari. 1999. Kinetics of visual pigment regeneration in excised mouse eyes and in mice with a targeted disruption of the gene encoding interphotoreceptor retinoid-binding protein or arrestin. *Biochemistry.* 38:12012–12019.
14. Saari, J. C., D. L. Bredberg, and D. F. Farrell. 1993. Retinol esterification in bovine retinal pigment epithelium: reversibility of lecithin:retinol acyltransferase. *Biochem. J.* 291:697–700.
15. Bernstein, P. S., and R. R. Rando. 1986. In vivo isomerization of all-*trans*- to 11-*cis*-retinoids in the eye occurs at the alcohol oxidation state. *Biochemistry.* 25:6473–6478.
16. McBee, J. K., V. Kuksa, R. Alvarez, A. R. de Lera, O. Prezhdo, F. Haeseleer, I. Sokal, and K. Palczewski. 2000. Isomerization of all-*trans*-retinol to *cis*-retinols in bovine retinal pigment epithelial cells: dependence on the specificity of retinoid-binding proteins. *Biochemistry.* 39:11370–11380.
17. Kaplan, M. W. 1984. Distribution and axial diffusion of retinol in bleached rod outer segments of frogs (*Rana pipiens*). *Exp. Eye Res.* 40:721–729.
18. Sears, R. C., and M. W. Kaplan. 1989. Axial diffusion of retinol in isolated frog rod outer segments following substantial bleaches of visual pigment. *Vision Res.* 29:1485–1492.
19. Azuma, K., M. Azuma, A. E. Walter, and T. P. Williams. 1991. Axial diffusion of all-*trans* retinol in single rods following bleach of rhodopsin. *Zoolog. Sci.* 8:431–436.
20. Chen, C., E. Tsina, M. C. Cornwall, R. K. Crouch, S. Vijayaraghavan, and Y. Koutalos. 2005. Reduction of all-*trans* retinal to all-*trans* retinol in the outer segments of frog and mouse rod photoreceptors. *Biophys. J.* 88:2278–2287.
21. Biernbaum, M. S., and M. D. Bownds. 1985. Frog rod outer segments with attached inner segment ellipsoids as an in vitro model for photoreceptors on the retina. *J. Gen. Physiol.* 85:83–105.
22. Spencer, M., P. B. Detwiler, and A. H. Bunt-Milam. 1988. Distribution of membrane proteins in mechanically dissociated retinal rods. *Invest. Ophthalmol. Vis. Sci.* 29:1012–1020.
23. Liebman, P. A., and G. Entine. 1968. Visual pigments of frog and tadpole (*Rana pipiens*). *Vision Res.* 8:761–775.
24. Imanishi, Y., M. L. Batten, D. W. Piston, W. Baehr, and K. Palczewski. 2004. Noninvasive two-photon imaging reveals retinyl ester storage structures in the eye. *J. Cell Biol.* 164:373–383.
25. Poo, M., and R. A. Cone. 1974. Lateral diffusion of rhodopsin in the photoreceptor membrane. *Nature.* 247:438–441.
26. Carslaw, H. S., and J. C. Jaeger. (1959) Conduction of Heat in Solids, 2nd Ed. Clarendon Press, Oxford, UK.
27. Tsukamoto, Y. 1987. The number, depth and elongation of disc incisures in the retinal rod of *Rana catesbeiana*. *Exp. Eye Res.* 45:105–116.
28. Crank, J. (1979) The Mathematics of Diffusion, 2nd Ed. Clarendon Press, Oxford, UK.
29. Ala-Laurila, P., A. V. Kolesnikov, R. K. Crouch, E. Tsina, S. A. Shukolyukov, V. I. Govardovskii, Y. Koutalos, B. Wiggert, M. E. Estevez, and M. C. Cornwall. 2006. Visual cycle: dependence of retinol production and removal on photoproduct decay and cell morphology. *J. Gen. Physiol.* 128:153–169.
30. Scandella, C. J., P. Devaux, and H. M. McConnell. 1972. Rapid lateral diffusion of phospholipids in rabbit sarcoplasmic reticulum. *Proc. Natl. Acad. Sci. USA.* 69:2056–2060.
31. Chen, C., Y. Jiang, and Y. Koutalos. 2002. Dynamic behavior of rod photoreceptor disks. *Biophys. J.* 83:1403–1412.
32. Daemen, F. J. 1973. Vertebrate rod outer segment membranes. *Biochim. Biophys. Acta.* 300:255–288.
33. Calvert, P. D., V. I. Govardovskii, N. Krasnoperova, R. E. Anderson, J. Lem, and C. L. Makino. 2001. Membrane protein diffusion sets the speed of rod phototransduction. *Nature.* 411:90–94.
34. Heck, M., S. A. Schadel, D. Maretzki, and K. P. Hofmann. 2003. Secondary binding sites of retinoids in opsin: characterization and role in regeneration. *Vision Res.* 43:3003–3010.
35. Schadel, S. A., M. Heck, D. Maretzki, S. Filipek, D. C. Teller, K. Palczewski, and K. P. Hofmann. 2003. Ligand channeling within a G-protein-coupled receptor. The entry and exit of retinals in native opsin. *J. Biol. Chem.* 278:24896–24903.
36. Liebman, P. A., and G. Entine. 1974. Lateral diffusion of visual pigment in photoreceptor disk membranes. *Science.* 185:457–459.
37. Blaurock, A. E., and M. H. Wilkins. 1972. Structure of retinal photoreceptor membranes. *Nature.* 236:313–314.
38. Zhou, Z., and E. Neher. 1993. Mobile and immobile calcium buffers in bovine adrenal chromaffin cells. *J. Physiol.* 469:245–273.
39. Dodson, C. S., A. V. Peresypkin, K. Rengarajan, S. Wu, and J. M. Nickerson. 2002. Diffusion coefficients of retinoids. *Curr. Eye Res.* 24:66–74.
40. Krasnovsky, A. A., Jr., and V. E. Kagan. 1979. Photosensitization and quenching of singlet oxygen by pigments and lipids of photoreceptor cells of the retina. *FEBS Lett.* 108:152–154.
41. Delmelle, M. 1978. Retinal sensitized photodynamic damage to liposomes. *Photochem. Photobiol.* 28:357–360.